NASA Technical Paper 2984

1990

Development and Approach to Low-Frequency Microgravity Isolation Systems

Carlos M. Grodsinsky
Lewis Research Center
Cleveland, Ohio

National Aeronautics and Space Administration
Office of Management
Scientific and Technical Information Division

Summary

The low-gravity environment provided by space flight has afforded the science community a unique arena for the study of fundamental and technological sciences. However, the dynamic environment observed on space shuttle flights and predicted for Space Station Freedom has complicated the analysis of prior "microgravity" experiments and prompted concern for the viability of proposed space experiments requiring long-term, low-gravity environments. Thus, isolation systems capable of providing significant improvements to this random environment are being developed. This report deals with the design constraints imposed by acceleration-sensitive, "microgravity" experiment payloads in the unique environment of space and a theoretical background for active isolation. A design is presented for a six-degree-of-freedom, active, inertial isolation system based on the baseline relative and inertial isolation techniques described.

Introduction

Interest in vibration isolation for microgravity experiments has increased within the microgravity science community as the space shuttle flight program has progressed and the small, but significant, levels of residual acceleration on the shuttle have become more widely recognized and documented (refs. 1 and 2). These residual accelerations result from several sources characteristic of the orbiting carrier and the orbital environment. Very-low-frequency (constant cycle to 10^{-3} Hz) accelerations due to drag, tidal effects, and gravity gradients contribute microacceleration levels g/g_o. (All variables and constants are defined in appendix A.) Orbiter thruster activity can contribute 10^{-4} to 10^{-2} g/g_o accelerations with significant duration, but these can be predicted and controlled. The most significant and troublesome contribution to most experiments is the moderate-frequency (10^{-3} to 100 Hz) dynamic spectrum of accelerations having magnitudes in the range 10^{-5} to 10^{-2} g/g_o. This dynamic background is primarily due to random excitations from manned activity on the orbiter as well as small thruster firings for orbit-keeping maneuvers. However, orbiter structure and flight systems also contribute observable intermittent and resonant accelerations to the background as the orbiter interacts with its dynamic mechanical and thermal environment.

To categorize the disturbances which are present in the space shuttle and which will be present in Space Station Freedom, the accelerations are grouped into three frequency ranges (ref. 3): (1) quasi-static external disturbances, (2) low-frequency vibration sources, and (3) medium- to high-frequency vibrations. The first category includes aerodynamic drag, gravity gradient effects, and photon pressure accelrations. The second category includes excitations due to large flexible space structures, crew motion, spacecraft attitude control, and robotic arms. The third catagory includes disturbances due to onboard equipment such as pumps and motors having a frequency range of about 10 Hz and higher. The range of accelerations observed on several shuttle missions or estimated for the accessible orbit is given in table I (refs. 1, 4, and 5).

The evolution of the Freedom Station design has led to potential limitations on long-term, low-gravity experimentation in this environment. It is now obvious that most of the true "microgravity" experiments will require isolation from this random milli-g environment if reproducible and useful results are to be expected. Because a large part of the transient disturbances have a frequency range from millihertz to 1 Hz, it is extremely difficult to design passive isolation systems with a resonance frequency of, at most, $1/\sqrt{2}$ times the lowest excitation frequency of interest, mainly the subhertz range. The serious limitation of passive isolators is the absence of materials which have useful ranges of both low modulus (providing low frequency) and appropriate damping (to avoid large-amplitude oscillation). Two-stage passive isolators can decrease the frequency range; however, limited damping leads to potentially unstable systems in the random excitation environment.

Passive isolation systems require extremely low stiffness for the isolation of small disturbance frequencies for typical values of mass associated with microgravity space experiments. In contrast, when there are direct disturbances to a payload, a small value of stiffness is not desirable. Thus, there is a tradeoff, and an optimal design would need to compensate for both direct disturbances, if present, and low-frequency base disturbances. Active systems offer significant advantages over passive systems in the orbital acceleration environment. This is due to the extremely small stiffnesses needed to isolate against such low-frequency base disturbances and the added capability needed to adapt to direct disturbances for the optimal isolation of a payload. In addition, since the responses to these

TABLE I.—ACCELERATION DISTURBANCES

Source	Acceleration, g/g_o	Frequency, Hz
Quasi-steady or constant cycle		
Aerodynamic drag	10^{-7}	0 to 10^{-3}
Light pressure	10^{-8}	0 to 10^{-3}
Gravity gradient	10^{-7}	0 to 10^{-3}
Periodic		
Thruster fire (orbital)	2×10^{-2}	9
Crew motion	2×10^{-3}	5 to 20
Ku-band antenna	2×10^{-4}	17
Nonperiodic		
Thruster fire (attitude)	10^{-4}	1
Crew pushoff	10^{-4}	1

two excitations require conflicting solutions, a closed-loop system is dictated for the control of both types of excitation disturbances.

Active systems require sensing of motion or position, and a feedback or feedforward control loop, or both, to counteract mechanical excitation and to minimize motion of an isolated body. Such systems introduce the complexity of a high-gain control system, but offer significant advantages in versatility and performance (ref. 4). To achieve a broad spectrum of isolation, both feedforward and feedback control loops are used in the isolation system design presented. This approach references the isolated payload to an inertial frame rather than to the dynamic support reference frame.

This report gives a theoretical background evaluation of both a fully magnetically suspended, one-degree-of-freedom system and a passive static support system (i.e., supported by a spring) with inertial electromagnetic damping. (A detailed description of the one-degree-of-freedom attractive relative suspension system appears in appendix B.) The fully magnetically suspended system was evaluated by using an attractive electromagnet, while the electromagnetically damped system was evaluated by using a Lorentz magnet. Magnetic systems of the attractive type have been used to suspend rotating shafts for a number of years, and the required negative feedback loops to control such systems have been discussed in numerous papers, giving the equivalent stiffness and damping coefficients for specific controllers (ref. 6). However, these studies have not treated the isolation of the suspended body from both direct and base excitations, and the response of such generic suspension systems to these types of disturbances has not been documented. In addition, designers of these rotating systems have not dealt with the inertial isolation of the rotating system or of the suspension environment, which could help reduce mechanical noise. Therefore, the dynamic response to base and direct disturbances of both systems has been evaluated.

Upon completion of this theoretical background development, the design of a prototype six-degree-of-freedom system based on both relative and inertial isolation techniques is presented. This prototype fulfills the broad spectrum of requirements produced by the dynamic environment for space-based experimentation.

Pictorial representations of both baseline systems evaluated are shown in figure 1, where each system is represented by an isolator between a base support and the isolated payload. The isolator is simply an actuator which is driven in proportion to certain feedback or feedforward signals, or both, depending on the desired response of the payload. For the attractive magnetic actuator, it is assumed that both the stiffness and the damping coefficient are derived from a relative position sensor. For the electromagnetic damping isolator, a Lorentz actuator is analyzed where the damping coefficient is derived from an inertial sensor and the stiffness is simply that of a passive spring. The background formulations of these systems have been separated in order to demonstrate the dynamic response of a payload to both relative and inertially based isolation systems. The six-degree-of-freedom inertial isolation design is based on a combination of both techniques.

The primary purpose of this activity is to use digital active control on dependent multidegrees of freedom. As part of the project, a six-degree-of-freedom system based on this prototype design will be tested under a full six-degree-of-freedom

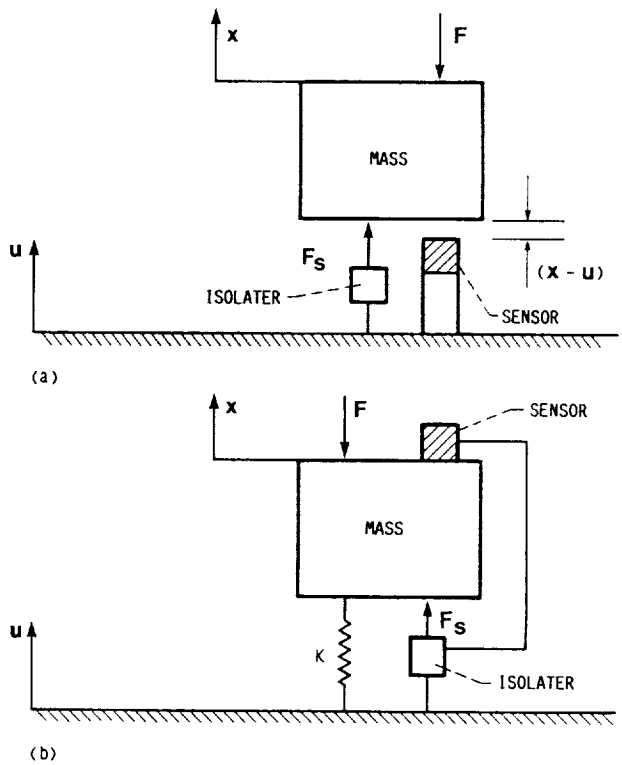

(a) Relative feedback system.
(b) Inertial damping system.

Figure 1.—Physical representation of active isolation systems.

free-fall condition on the NASA Lewis Learjet to acquire the coupled response between all six degrees of freedom in a low-gravity environment.

Theory and Formulation of Baseline Systems

The active isolators described in this report are effective at frequencies above 0.01 to 0.1 Hz. This constraint arises not from technology limitations, but from practical limitations on the stroke needed to isolate against the very low frequencies. Volume constraints in the shuttle and in the future Freedom Station manned environment laboratory modules limit the stroke of any support system. Aerodynamic drag, for example, acts on a solar-pointing station with a frequency equal to that of the orbital frequency (about 90 min per orbit). Although drag is a function of the atmospheric conditions during a specific mission, an average g/g_o of 10^{-7} will be used. Thus, the distance Freedom Station would travel under such an acceleration would be $2(a/\omega^2)$, or 1.5 m (4.7 ft), where $\omega=2\pi/(90\times60)$ rad/sec and $a=(9.81\ \text{m/sec}^2)\times(10^{-7}\ g/g_o)$, not including initial conditions. Thus, an isolated payload would be forced to follow such a large spacecraft displacement, but be active in a much smaller region. This active region would depend on the volume constraints of a payload in the shuttle or in the Freedom Station microgravity module.

The following two baseline cases assume the use of an attractive electromagnet and a Lorentz force actuator, respectively, and can be analyzed as spring-mass-damper systems. It is assumed that the spring and damper characteristics for the attractive electromagnet and the damping characteristics for the Lorentz actuator are actively controlled and translated into actuator response by a control law dependent on the response characteristics desired. Using an attractive electromagnetic actuator, one can produce forces in only one direction. Therefore, to achieve a push-pull configuration one needs to use two apposing electromagnets acting on an armature. Figure 2 illustrates the two general magnetic actuator configurations: the attractive electromagnet and the Lorentz force actuator. For the attractive electromagnetic actuators, the force produced by one magnet is proportional to the square of the current and inversely proportional to the square of the gap. Figure 3 shows the magnetic circuit actuator's squared dependence on current. Because of these nonlinear characteristics, a bias current linearization technique is used. Thus, the bias current i_b is used to produce a nearly linear control law such that, for small disturbances about this current, the control force produced can be assumed linear. In order to control this system, one must close a control loop around position and velocity feedback signals with a bias current to work in the more linear regime of the force-versus-current plot of a magnetic circuit, as shown in figure 3. Other nonlinearities due to hysteresis and saturation arise between

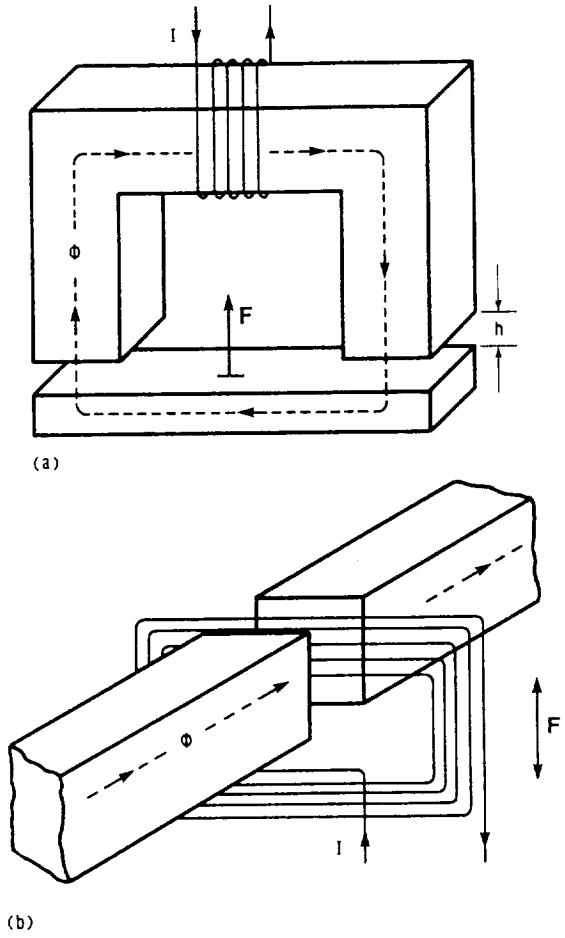

(a) Attractive electromagnetic actuator.
(b) Lorentz force actuation.

Figure 2.—General magnetic actuator configurations.

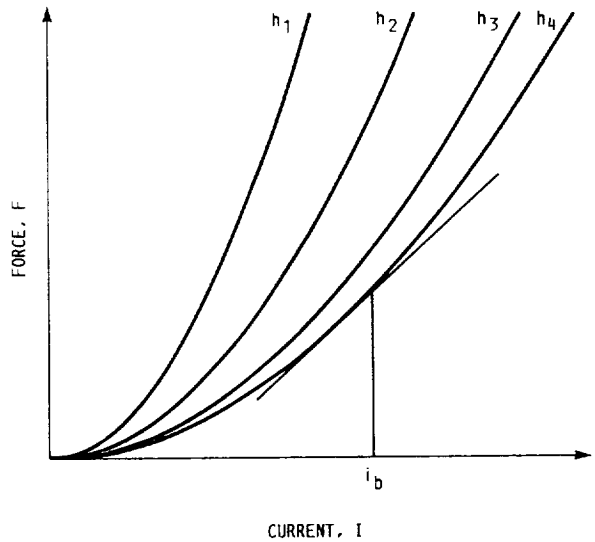

Figure 3.—Squared dependence of magnetic-circuit actuator on current (i_b is bias current; gap $h_1 < h_2 < h_3 < h_4$).

magnetic flux and input coil current, but are not significant with proper care of the system design.

In contrast, the Lorentz actuator can produce forces bi-directionally. The force produced by a Lorentz actuator is a vector quantity equal to the cross product of current and field ψ. Therefore, depending on the direction of current flow in the coil, one can produce a force in either a positive or negative direction. Because of this actuator's linear dependence on control current, linearization is not needed, and this actuator is open-loop stable. The Lorentz actuator thus has advantages over the magnetic circuit actuator, but requires more power to produce a certain force than does the magnetic circuit configuration. However, the forces needed to control a payload in the "weightless" environment of space are small, and this inefficiency is not as limiting as on the Earth.

The basic concept behind these active feedback isolation techniques is to sense position, velocity, acceleration, or velocity and acceleration, and then to drive an actuator 180° out of phase with this signal in order to cancel a disturbance to the payload. If there is knowledge about certain disturbances, a feedforward loop can anticipate an excitation and react without an error signal. Thus, the optimal dynamic response for microgravity experiments to known and sensed orbiter environments would result from the inertial isolation of a body by a feedforward/feedback type controller. Such a controller does not circumvent the need for relative information of the payload in order to follow the large motion disturbances without exceeding boundary conditions (i.e., volume constraints). These active isolation techniques can be implemented by using either analog or digital control schemes to close the feedback and feedforward control loops.

Base Disturbance Formulations for Baseline Systems

The responses of the magnetic circuit isolator and the Lorentz electromagnetically damped system in one degree of freedom are evaluated by their transmissibilities and effectiveness in isolating against both base and direct disturbances. To summarize, these transmissibilities and effectiveness functions are given with a brief description of their formulation. (Appendix C gives a detailed analysis of the transmissibility and effectiveness formulations and their results for a variety of feedback schemes.) First, the responses, or transmissibilities, of both systems are generated for harmonic base excitations by using the active isolation system's differential equations of motion. These equations of motion are formulated by using Newton's first and second laws, where the base displacement $\mathbf{u}$ is actually a time function, so that $\mathbf{u} = \mathbf{u}(t)$. The same is implied for a directly applied force such that, in actuality, $\mathbf{F} = \mathbf{F}(t)$. Therefore, for a spring-mass-damper system, the equations of motion for base excitation become, for the magnetic circuit isolator,

$$m\frac{d^2\mathbf{x}}{dt^2} + k_{eq}(\mathbf{x}-\mathbf{u}) + c_{eq}\left(\frac{d\mathbf{x}}{dt} - \frac{d\mathbf{u}}{dt}\right) = 0 \qquad (1)$$

and for the electromagnetic damping isolator,

$$m\frac{d^2\mathbf{x}}{dt^2} + c\frac{d\mathbf{x}}{dt} + K\mathbf{x} = K\mathbf{u} \qquad (2)$$

These systems look very similar to passive viscoelastic systems with the exception that, for all practical purposes, both the stiffness and damping of either isolator can be set as desired. By joining these control methods appropriately, one can produce an active system with variable stiffness and damping referenced to inertial space. Therefore, these systems can easily be configured as adaptive systems where, by using sensed information from the disturbance environment, the control law can be changed to optimize the isolation of the payload. In the magnetic circuit actuator, the stiffness and damping are not strictly independent, but the dependence is minimal if certain control parameters are met. (For example, a certain amount of damping is needed in order to overcome instabilities.)

Baseline System Response to Base Disturbances

In defining the dynamic base motion equations for both systems, the stiffness and damping terms can be found by using the appropriate control law needed for a stable negative feedback system. The stiffness and damping solutions for both baseline cases are presented in appendixes B and C. In summary, the stiffness coefficient for the magnetic circuit becomes

$$k_{eq} = k_\theta + \frac{k_i k_a k_p\left[k_g(1-\tau_2\tau_1\omega^2)+(k_g+k_r)(\tau_2+\tau_1)\tau_2\omega^2\right]}{(1-\tau_2\tau_1\omega^2)^2+(\tau_2+\tau_1)^2\omega^2} \qquad (3)$$

For the electromagnetic isolator, because the mass is being statically supported by a passive spring, the stiffness is simply K. By summarizing the damping coefficients for both isolators, the magnetic circuit damping coefficient becomes

$$c_{eq} = \frac{k_i k_a k_p\left[(1-\tau_2\tau_1\omega^2)(k_g+k_r)\tau_2 - k_g(\tau_2+\tau_1)\right]}{(1-\tau_2\tau_1\omega^2)^2+(\tau_2+\tau_1)^2\omega^2} \qquad (4)$$

and the electromagnetic damping coefficient is

$$c = -\psi N I_{avv} \qquad (5)$$

where $I_{avv} = E_{avv}/R$ (Note: calculations assume negligible inductance.) The magnetic circuit actuator system is more complex than the Lorentz actuator because of the nonlinear characteristics of the magnet. Also, since the stiffness is a function of the excitation frequency, the natural frequency of this system is not constant. However, for small excitation frequencies, the natural frequency of the system can be assumed to be constant.

In order to solve the equations by defining the base excited system transfer function, as in appendix C, the dynamic equations are transformed into the frequency domain by using the Laplace transformation:

$$F(s) = \int_{-\infty}^{\infty} F(t)e^{-st}dt \tag{6}$$

Then, by transforming the transfer functions into the frequency domain, the two equations become, for the magnetic circuit system,

$$\frac{X}{U}(s) = \frac{2\xi\omega_n s + \omega_n^2}{s^2 + 2\xi\omega_n s + \omega_n^2} \tag{7}$$

and for the electromagnetic damping system,

$$\frac{X}{U}(s) = \frac{\omega_n^2}{s^2 + 2\xi\omega_n s + \omega_n^2} \tag{8}$$

The frequency response for both functions is obtained from the relation

$$\frac{X}{U}(j\omega) = \lim_{t\to\infty}\left[\frac{X}{U}(s)\right] \tag{9}$$

where $j = \sqrt{-1}$, and $s = j\omega$. Thus, the transfer functions in terms of frequency response are vectors in the complex plane. The magnitude of vibration measured on the isolated payload resulting from a sinusoidal excitation $\mathbf{u}(t) = B\sin(\omega t)$ is the vector length of $X(j\omega)/U(j\omega)$. This value, a scalar, is called the transmissibility function of the system. The transmissibility is generally written as $T = |(X/U)(j\omega)|$.

Therefore, the transmissibility functions become, for the magnetic circuit system,

$$T = \left|\frac{X}{U}(j\omega)\right| = \left\{\frac{1 + \left(2\xi\frac{\omega}{\omega_n}\right)^2}{\left[1 - \left(\frac{\omega}{\omega_n}\right)^2\right]^2 + \left(2\xi\frac{\omega}{\omega_n}\right)^2}\right\}^{1/2} \tag{10}$$

and for the electromagnetic damping system,

$$T_{av} = \left|\frac{X}{U_{av}}(j\omega)\right| = \frac{1}{\left\{\left[1 - \left(\frac{\omega}{\omega_n}\right)^2\right]^2 + \left(2\xi\frac{\omega}{\omega_n}\right)^2\right\}^{1/2}} \tag{11}$$

By plotting these transmissibilities, one can see the effect of changing the stiffness or damping of either system. The transmissibility curve for the first case, shown in figure 4, illustrates the effect of increasing the damping coefficient of the magnetic circuit isolator system. The curves show that with enough velocity feedback gain k_r the system can become overly damped. This gives rise to a well-damped resonance but less isolation at excitation frequencies above $\sqrt{2}\omega_n$ than would be achieved with a less damped system. Increasing or decreasing the position gain k_g shifts the natural frequency of the system to the right or left because of the change in equivalent stiffness.

The effect of increasing the damping coefficient of the Lorentz electromagnetic damping system is illustrated in figure 5. The curves show the response of the system to increased velocity feedback (i.e., damping) determined from the integration of an inertial sensor signal. The advantage of

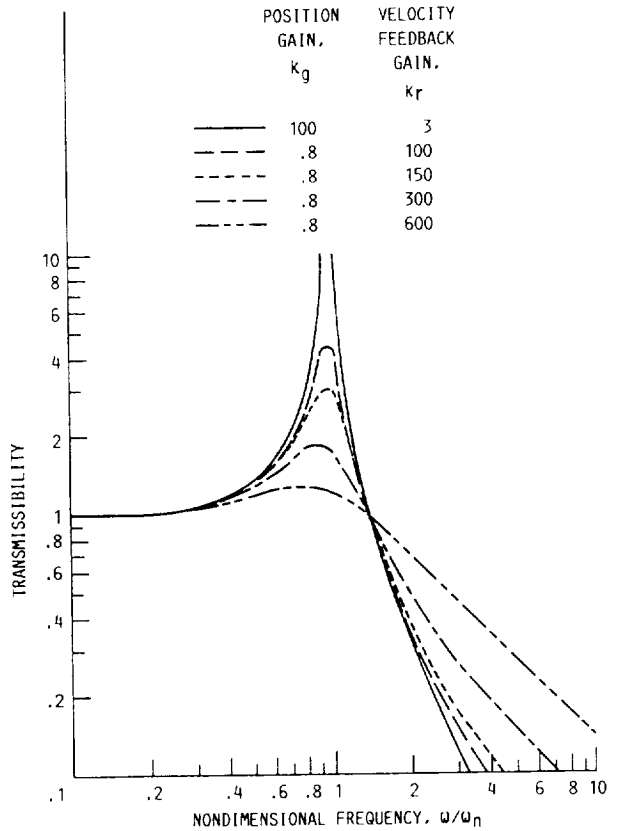

Figure 4.—Relative feedback transmissibility curves ($k_g > 0.5198$, current stiffness $k_i > 0.01144$).

active damping derived from an inertial reference is that it removes the resonant response, broadening and smoothing the transition between the low-frequency and high-frequency regions, while reducing both the transmission and the response, particularly in the low-frequency range of interest. The effect of such a system for large values of velocity feedback gain can be understood by noting that it is equivalent to having a passive damper attached between the isolated mass and a virtual inertial reference. As the damping is increased, the isolated mass becomes more and more tightly coupled to the (motionless) ideal inertial reference. In other words, the stronger the damping, the better the isolation. This type of response is not seen in the pure suspension case because the velocity term was determined from the derivative of a relative position sensor, giving rise to the response shown in figure 4.

In order to relate these curves to the microgravity environment, one can use a g/g_o-versus-frequency plot, which was generated from typical Microgravity Science Laboratory (MSL) acceleration data (refs. 1 and 2) measured on a shuttle flight, and superimpose the transmissibility curves on this data to predict the isolation performance achievable for such disturbances. By superimposing these curves, one can get a rough idea of the capability of such a system in isolating against such low-frequency disturbances. These curves are presented in figure 6 (refs. 1 and 3). The figure shows selected peak accelerations (open data points) typical of those observed on shuttle missions (refs. 1 and 3) and an upper bound (line with positive slope) that is intended to reflect the worst-case limit for such an environment. The solid data points show the effect of attenuating these mechanical disturbances through the Lorentz isolator and the resultant worst-case line.

Direct Disturbance Formulations for Baseline Systems

As explained in the preceding section, the curves in figures 4 to 6 all demonstrate system response to base excited harmonic motions. However, disturbances may also be generated directly on the payload itself. The sensitivity of the isolated payload to a direct disturbing force is characterized by a term called the isolated payload mobility. The mobility of the payload is the vector magnitude of $X(s)/F(s)$. This parameter measures the amplitude of the payload deflection per unit of force amplitude. For direct disturbance only, the equations of motion for both systems, are, for the magnetic circuit system,

$$m\frac{d^2\mathbf{x}}{dt^2} = \mathbf{F}(t) - k_{eq}\,\mathbf{x} - c_{eq}\frac{d\mathbf{x}}{dt} \tag{12}$$

and for the electromagnetic damping system,

$$m\frac{d^2\mathbf{x}}{dt^2} = \mathbf{F}(t) - K\mathbf{x} - c\frac{d\mathbf{x}}{dt} \tag{13}$$

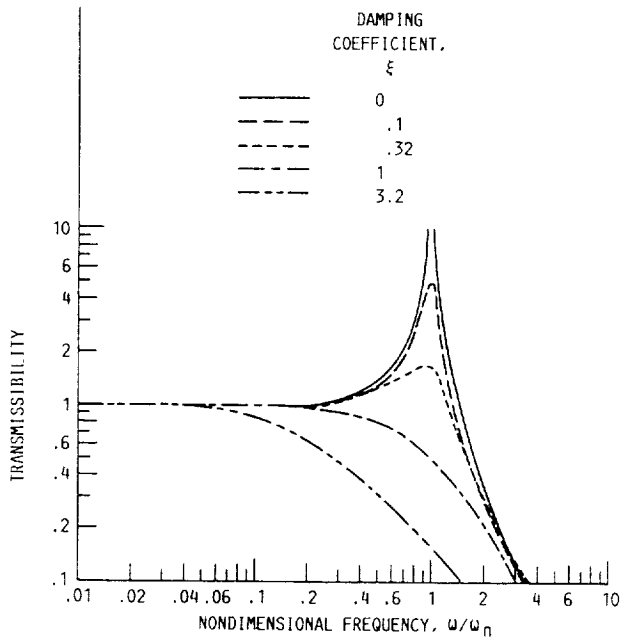

Figure 5.—Inertial damping transmissibility curves.

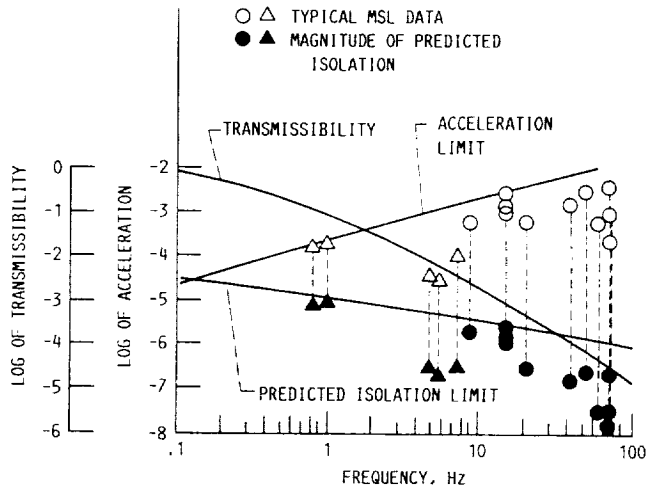

Figure 6.—Inertial damping transmissibility curve superimposed on Microgravity Science Laboratory (MSL) acceleration data and predicted acceleration response for two locations on the space shuttle.

Baseline System Response to Direct Disturbances

Equations (12) and (13) can be placed in the Laplace operator format, and from the definition of the vector magnitude $X(s)/F(s)$, the mobility equations for both cases are, for the magnetic circuit system,

$$\frac{X(s)}{F(s)} = \frac{1}{ms^2 + c_{eq}s + k_{eq}} \tag{14}$$

and for the electromagnetic damping system,

$$\frac{X(s)}{F(s)} = \frac{1}{ms^2 + cs + K} \tag{15}$$

In order to evaluate the effectiveness of these active systems, the ratio of $X(s)/F(s)$ for the active system to $X(s)/F(s)$ for a typical passive system is used. This ratio is called the mobility effectiveness $X_f(s)$. Therefore, if $X_f(s)$ is unity, then the active system behaves the same as the passive one. If $X_f(s)$ is zero, then no motion of the payload results from a finite applied force. If $X_f(s)$ is greater than unity, then the active system amplifies the effect of the applied force, increasing the payload motion. The equations for the mobility effectiveness function for both cases, in terms of frequency response, where the vector length of $X_f(s)$ is $|X_f(j\omega)|$, are as follows: for the magnetic circuit system,

$$\left| X_f\left(\frac{j\omega}{\omega_n}\right) \right| = \frac{\omega_n}{\omega_{na}} \left\{ \frac{\left[1 - \left(\frac{\omega}{\omega_n}\right)^2\right]^2 + \left(2\xi_1 \frac{\omega}{\omega_n}\right)^2}{\left[1 - \left(\frac{\omega}{\omega_n}\right)^2\right]^2 + \left(2\xi \frac{\omega}{\omega_n}\right)^2_a} \right\}^{1/2} \tag{16}$$

where for small excitation frequencies $\omega_{na} \approx \omega_n$, active $\omega_n = (k_{eq}/m)^{1/2}$, and $c_{eq}/m = 2\xi\omega_n$, and for the electromagnetic damping system,

$$\left| X_f\left(\frac{j\omega}{\omega_n}\right)_v \right| = \left\{ \frac{\left[1 - \left(\frac{\omega}{\omega_n}\right)^2\right]^2 + \left(2\xi_1 \frac{\omega}{\omega_n}\right)^2}{\left[1 - \left(\frac{\omega}{\omega_n}\right)^2\right]^2 + \left(2\xi \frac{\omega}{\omega_n}\right)^2} \right\}^{1/2} \tag{17}$$

where $c/m = 2\xi\omega_n$, $\omega_n = (K/m)^{1/2}$, $\xi = \frac{1}{2} G_v (1/Km)^{1/2}$, and $c = G_v$. In equations (16) and (17), ξ_1 is the damping coefficient of a passive spring and has a value of 0.05.

The effectiveness functions are plotted in figures 7 and 8. The figures present the effectiveness of the active-feedback, force-actuated vibration isolation systems as compared with a passive system with a critical damping coefficient of 0.05, which is typical for passive systems of the type used with low-frequency system resonances.

Six-Degree-of-Freedom Prototype Development

As shown by the transmissibility curves in figures 4 and 5, there are many advantages in developing isolation systems with the specific characteristics of both active relative and inertial closed-loop isolation systems. Systems which exploit inertial damping methods have been developed; however, they are limited by the cutoff frequencies obtainable because of the passive stiffness used for static support of the payload. Such

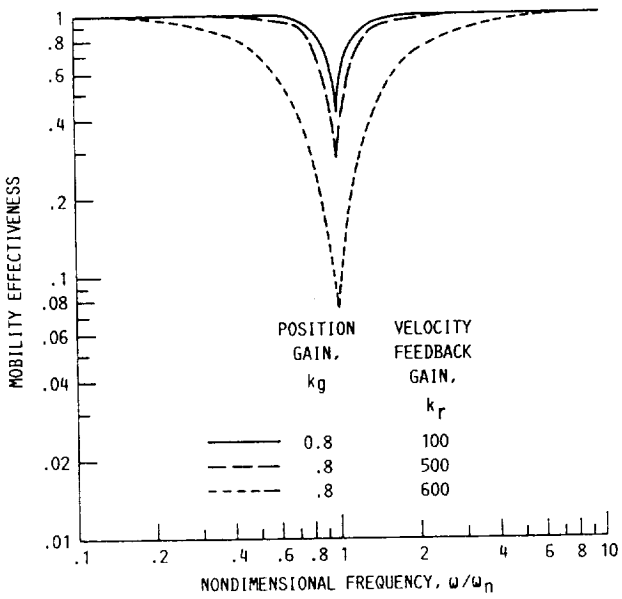

Figure 7.—Relative feedback mobility effectiveness curves.

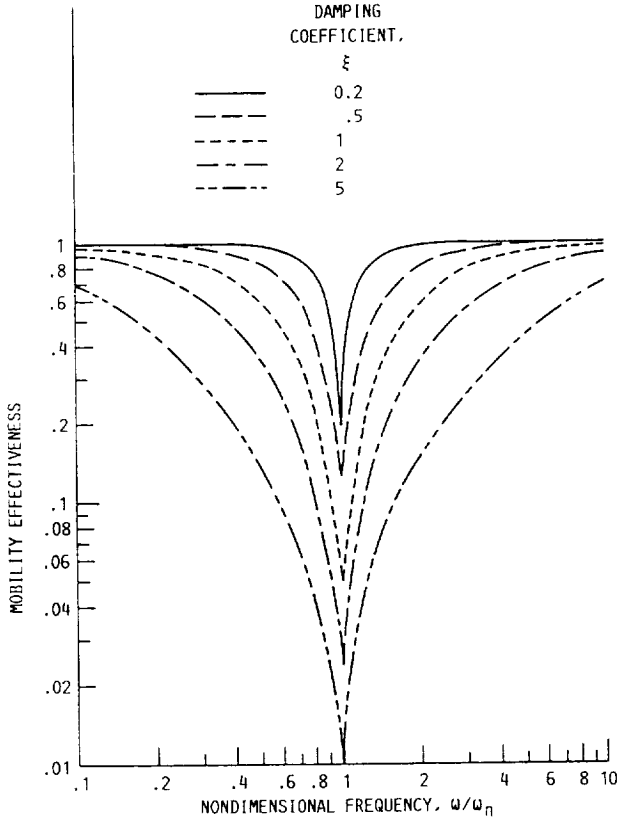

Figure 8.—Inertial damping mobility effectiveness curves.

a passive stiffness can be physically described in terms of a classical spring where the stiffness must be large enough to support the constant loading a payload experiences. This required stiffness dictates the dynamic stiffness of the system, once a transient disturbance is introduced. However, by actively supporting the payload with an integral term of the relative position, and by setting the relative position gain term appropriately, one can tailor the effective dynamic stiffness of a system to whatever value is desired, depending on the user's requirements. In effect, one can design an active support system with classical isolation characteristics with the versatility of changing the dynamic stiffness and damping parameters independently to produce a desired response. This gives the ability to set the cutoff frequency of such a system to much lower values, if the appropriate strokes are obtainable in the working volume of the payload. However, for such a relative sensor defined control system, increasing the damping gain term gives better response at resonance, but impedes isolation at frequencies above $\sqrt{2}\omega_n$. This response arises from obtaining the damping coefficient of the system from a relative velocity, which manifests itself in the $2\xi\omega/\omega_n$ term in the numerator of equation (10), shown in figure 4.

In developing the appropriate control logic for optimal payload isolation, an accelerometer referenced to the moving frame is joined with a relative sensor, which is needed for support, in a feedforward capacity. By adding the appropriate number of integrals of the inertial sensor to the appropriate relative information, one can obtain the inertial isolation response shown in figures 5 and 8 nonintrusively. Isolating in such a manner, one can configure a system independent of the actual payload, and by digitally controlling such a system, the appropriate parameters can be programmed for specific requirements.

In order to expand on these baseline isolation techniques, one can design a one-degree-of-freedom isolator with a large enough stroke to accommodate the payload motion needed in one direction. However, in reality, one needs to accommodate the translations and rotations in three-dimensional space. Therefore, a prototype six-degree-of-freedom system was designed with at least 0.762 cm (0.3 in.) possible displacement in three translations at the actuator locations.

The translational dimensions and the physical layout of the system used can be scaled to meet a variety of isolation and integration requirements. The design described here is one concept at a physical layout of a six-degree-of-freedom system based on a feedforward/feedback controller described in the baseline development. This prototype design uses attractive electromagnets as the force-generating devices rather than the linear Lorentz force magnets, in order to compensate for the greater support necessitated by the 1-g field in the laboratory environment. A layout of the physical system is shown in figure 9, where the hexagonal platform is the isolated payload. This system was designed for use in a laboratory environment; therefore, the magnets are larger than would be needed in a space-based system. The electromagnets designed have a

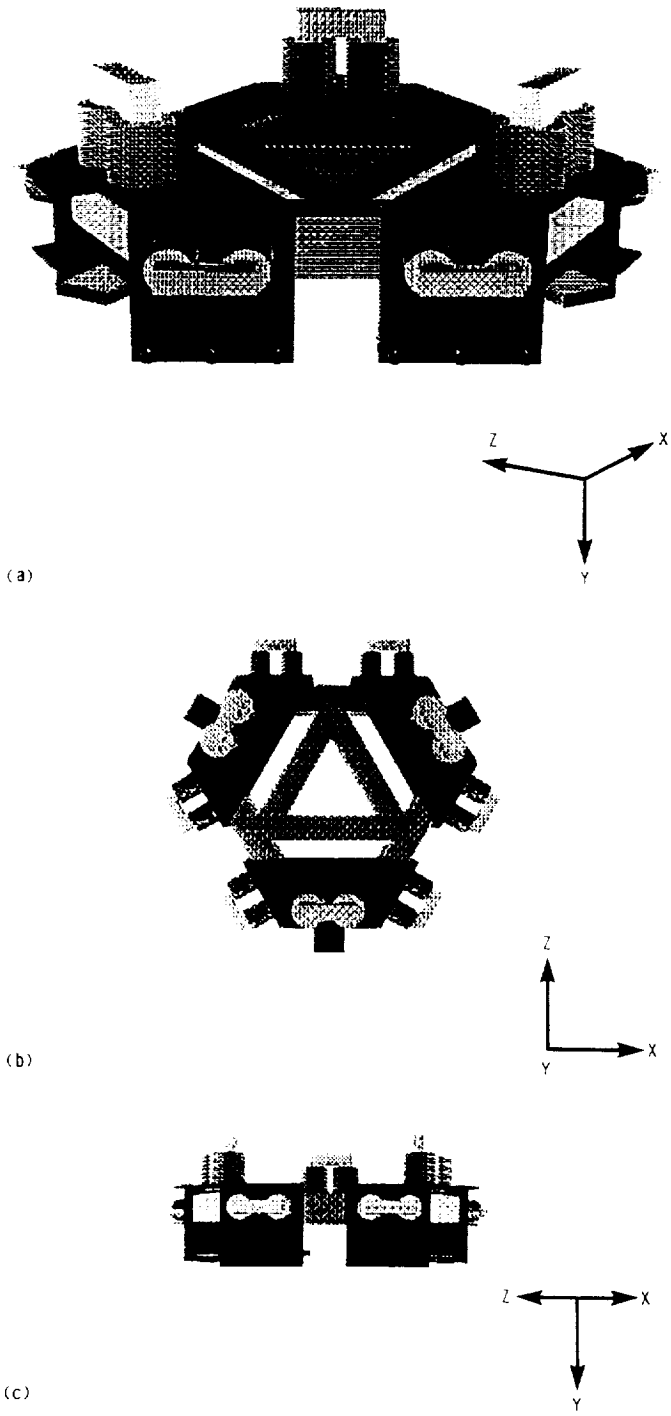

(a) Perspective view.
(b) Top view.
(c) Side view.

Figure 9.—Nonintrusive inertial isolation system layout.

suspension capability, at 4 A and 0.318 cm (0.125 in.) gap, of about 444.822 N (100 lb) each. Since these actuators are attractive, a total of 12 would be needed for control of all 6 degrees of freedom. However, for expediency in hardware fabrication, only nine are used in the laboratory prototype.

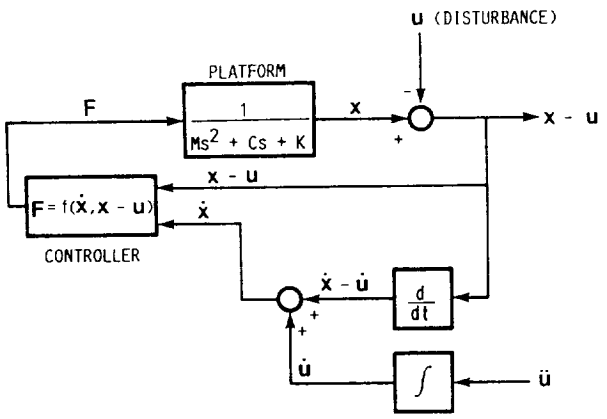

Figure 10.—One-degree-of-freedom inertial control system.

Gravity acts as the restoring force in the vertical direction. Presently the triaxial actuators are controlled independently. The relative motion of the payload with respect to the dynamic support structure and the inertial acceleration of the dynamic structure are measured at each of the three triaxial actuator locations.

Summarizing this nonintrusive inertial isolation control approach in one direction, one can see that the equation of motion for a typical suspension configuration, equation (1), must be changed to have the following form:

$$m\frac{d^2\mathbf{x}}{dt^2} + k_{eq}(\mathbf{x}-\mathbf{u}) + c_{eq}\left(\frac{d\mathbf{x}}{dt}\right) = 0 \qquad (18)$$

To design a system with the equivalent equation of motion shown in equation (18), one must configure the closed-loop control system around both the relative and inertial motion of the dynamic support structure. By using this information as the feedback/feedforward control signals, one arrives at the following equation of motion for such a system:

$$m\frac{d^2\mathbf{x}}{dt^2} + k_{eq}(\mathbf{x}-\mathbf{u}) + c_{eq}\left(\frac{d\mathbf{x}}{dt} - \frac{d\mathbf{u}}{dt}\right) + c_{eq}\left(\frac{d\mathbf{u}}{dt}\right) = 0 \qquad (19)$$

The control block diagram for this control system is shown in figure 10.

Concluding Remarks

The active magnetic systems described here have advantages over passive isolators because of their ability to isolate against the low frequencies present on the orbital carriers, as well as their ability to implement an adaptive control to isolate against both the direct and base excitations present in all pressurized modules. Therefore, the optimal isolation of microgravity science payloads will require an adaptive digitally controlled system to optimize isolation coefficients to most effectively prevent disturbances from perturbing the payload. To lower the corner frequencies of such an active system, one would need to use actuators with larger strokes. However, because of the volume constraints present in space flight vehicles, an isolated payload will have to follow these very low steady-state accelerations resulting from aerodynamic drag, gravity gradient effects, and other factors. To achieve the microgravity requirements suggested by the Microgravity Sciences and Applications Division for the Freedom space station for any significant length of time, microgravity vibration isolation will have to become a systems-engineered solution as well as an experiment-specific concern. Thus, the requirements for acceleration-sensitive microgravity space experiments will dictate multistage isolation concepts which will combine both passive and active systems, where the control of the center of gravity of Freedom Station will be closed around such microgravity steady-state accelerations.

Lewis Research Center
National Aeronautics and Space Administration
Cleveland, Ohio, February 28, 1990

Appendix A
Symbols

A	cross-sectional area of magnetic pole face
a	average acceleration of gravity on the Earth's surface, 9.81 m/sec^2
B	peak amplitude
b_2	servo force per payload mass
c	inertial electromagnet damping coefficient, N-sec/m
c_{eq}	relative electromagnet damping coefficient, N-sec/m
E_{avv}	accelerometer voltage output, V
$\mathbf{F}$	direct disturbance, N
$\mathbf{F}_s$	isolator force, N
F_o	force due to gravity on a system of mass m
F_p	force exerted by magnetic pole face
f_o	accelerometer's natural frequency
G_v	inertial velocity feedback gain term
g	acceleration, m/sec^2
g_o	acceleration due to Earth's gravitational field, m/sec^2
h	air gap between pole face and armature
h_o	static equilibrium gap length
I_{avv}	electromagnet current, α velocity
i	current through a coil
i_b	magnetic circuit current bias
K	passive stiffness coefficient, N/m
k_a	magnetic circuit current amplifier stiffness
k_{eq}	magnetic circuit isolator stiffness, N/m
k_g	magnetic circuit position gain
k_i	magnetic circuit current stiffness
k_p	magnetic circuit sensor amplifier gain
k_r	magnetic circuit velocity feedback gain
k_θ	magnetic circuit position stiffness
l	length of pivoted beam
l_1	actuator location from pivot point
m	mass, kg
N	number of ampere turns
R	resistance, Ω
T	transmissibility
t	time, sec
$\mathbf{u}$	position of base
v	velocity, m/sec
$X_f(s)$	mobility effectiveness
$\mathbf{x}$	position of payload
θ	angular displacement
μ_o	permeability of free space, $4\pi \times 10^{-7}$ H/m
v_c	control voltage
v_p	proportional feedback voltage
ξ	active damping coefficient
ξ_1	passive damping coefficient
τ_1	time constant of sensing circuit
τ_2	time constant of differentiator
ϕ	magnetic flux
ψ	magnetic field strength
ω	excitation frequency
ω_n	system resonance frequency
ω_{na}	active system resonance frequency

Appendix B
One-Degree-of-Freedom Magnetic Circuit Actuator Suspension

The purpose of this appendix is to support the summary of the attractive relative suspension system presented as background for the prototype feedforward/feedback isolation system. The formulations of the relative suspension equations for an isolation system are very similar to equivalent formulations for rotating magnetic bearing systems. Such derivations can also be found in many papers on the subject of magnetic bearings (e.g., ref. 6).

In analyzing a one-degree-of-freedom, attractive, relative magnetic actuator suspension system, as shown in figure 11, small motions are assumed about some center position so that a linearized approach can be taken. Also, the flux levels in the core and armature of the electromagnetic circuit are assumed to be below saturation. The total magnetic flux in an air gap (ref. 6) is

$$\phi = \frac{\mu_o A N i}{h} \tag{B1}$$

Without considering leakage and fringe effects in the magnet, the force exerted by the magnet is

$$F_p = \frac{\phi^2}{2\mu_o A} \tag{B2}$$

Therefore, substituting the relation for the magnetic flux in an air gap gives the relation

$$F_p = \frac{\mu_o A N^2 i^2}{2h^2} \tag{B3}$$

For both air gaps, the total force exerted is thus

$$F = 2F_p = \frac{\mu_o A N^2 i^2}{h^2} \tag{B4}$$

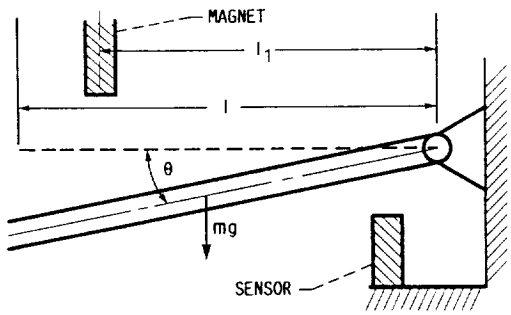

Figure 11.—Physical description of one-degree-of-freedom relative isolation system.

Then the actual gap h and current i, for the system shown in figure 11, have the form

$$h = h_o - l_1\theta \tag{B5}$$

$$i = i_b + \Delta i \tag{B6}$$

The negative sign occurs in h because as the mass of the system moves up, the clearance in the gap decreases. Therefore, substituting these relations for h and i into the force relation for an electromagnetic circuit gives the following equation:

$$F = \frac{\mu_o A N^2 (i_b + \Delta i)^2}{(h_o - l_1\theta)^2} \tag{B7}$$

By assuming that both $l_1\theta$ and Δi are small, equation (B7) can be approximated by a binomial expansion about the bias current i_b and the gap h. This then gives a linear relationship between the force F and Δi, and makes it possible to use a linear control scheme. The binomial expansion of equation (B7) becomes

$$F = \frac{\mu_o A N^2 i_b^2}{h_o^2}\left(1 + \frac{2l_1\theta}{h_o} + \frac{2\Delta i}{i_b}\right) \tag{B8}$$

The static equilibrium equation for the one-degree-of-freedom system as shown in figure 11 becomes

$$mg\,\frac{l}{2} = F_o l_1 \tag{B9}$$

Thus,

$$F_o = mg\,\frac{l}{2l_1} = \frac{\mu_o A N^2 i_b^2}{h_o^2} \tag{B10}$$

Then, by setting Δi in the linearized force equation equal to zero, one arrives at

$$F = mg\,\frac{l}{2l_1} - k_\theta \theta l_1 = \frac{\mu_o A N^2 i_b^2}{h_o^2} + \frac{2\mu_o A N^2 i_b^2 \theta l_1}{h_o^3} \tag{B11}$$

Therefore, the position stiffness is, from equation (B11),

$$k_\theta = -\frac{2\mu_o A N^2 i_b^2}{h_o^3} \tag{B12}$$

A position displacement θl_1 toward the magnet increases the force in that same direction. An actual spring would apply a force tending to restore the initial position of the beam at h_o. Now setting θ in the linearized force equation equal to zero gives a linearized force component proportional to the bias current. This has been called a current stiffness (ref. 6); however, a change in Δi does not tend to restore the beam to its original position, but an increase in current does tend to force the beam away from its steady-state value always towards the magnet. The following relation demonstrates this proportionality constant which arises from linearizing the force around a bias current:

$$F = mg\frac{l}{2l_1} - k_i\Delta i = \frac{\mu_o AN^2 i_b^2}{h_o^2} + \frac{2\mu_o AN^2 i_b \Delta i}{h_o^2} \tag{B13}$$

Therefore, this proportionality constant becomes

$$k_i = -\frac{2\mu_o AN^2 i_b}{h_o^2} \tag{B14}$$

The dynamic equation for the system of interest can be written as

$$mg\frac{l}{2l_1} + \Delta F = \frac{\mu_o AN^2 i_b^2}{h_o^2} + k_i\Delta i + ml_1\frac{d^2\theta}{dt^2} + k_\theta\theta l_1 \tag{B15}$$

Since, from the static equilibrium case, F_o was set equal to the force needed to support the beam at its equilibrium position,

$$F_o = mg\frac{l}{2l_1} = \frac{\mu_o AN^2 i_b^2}{h_o^2} \tag{B16}$$

then the dynamic equation of this system around its static equilibrium position, which is set by the amount of bias current, can be represented by

$$\Delta F = k_i\Delta i + ml_1\frac{d^2\theta}{dt^2} + k_\theta\theta l_1 \tag{B17}$$

By assuming that the current $i = i_b + i_c$, where i_b is the bias current and i_c is the control current, then $\Delta i = i_c$. And assume that at equilibrium, or at $\theta = 0$, $h = h_o$. The dynamic response equation then becomes

$$\Delta F = k_i i_c + ml_1\frac{d^2\theta}{dt^2} + k_\theta\theta l_1 \tag{B18}$$

In order to stabilize the system, one needs to take the derivative of the position signal and use both position and velocity to control the system. This portion of the control

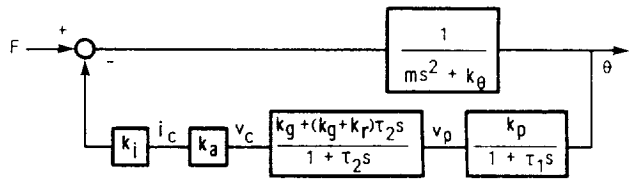

Figure 12.—Control block diagram.

circuit can be modeled as a position constant k_g and a velocity constant k_r. These gains are adjustable and affect the stiffness and damping coefficients acting on the system. The transfer function of this portion of the circuit can be modeled as

$$\frac{v_c}{v_p} = k_g + \frac{k_r\tau_2 s}{1+\tau_2 s} \tag{B19}$$

$$= \frac{k_g + (k_g + k_r)\tau_2 s}{1+\tau_2 s} \tag{B20}$$

Then current amplification is described by a constant as follows:

$$\frac{i_c}{v_c} = k_a \tag{B21}$$

A block diagram can be formed, as shown in figure 12, with force as the input and position as the output. The transfer function becomes

$$\frac{\theta}{F}(s) = \frac{\dfrac{1}{ms^2 + k_\theta}}{1 + \dfrac{1}{ms^2 + k_\theta}\left\{\dfrac{k_i k_a k_p |k_g + (k_g + k_r)\tau_2 s|}{(1+\tau_2 s)(1+\tau_1 s)}\right\}} \tag{B22}$$

In order to determine the theoretical stiffness and damping coefficients, the dynamic equations of the one-degree-of-freedom system are written and compared with a lumped second-order model. By using the block diagram (fig. 12), an equation involving position θ and control current i_c can be written as follows:

$$i_c = \theta\frac{k_a k_p |k_g + (k_g + k_r)\tau_2 s|}{(1+\tau_2 s)(1+\tau_1 s)} \tag{B23}$$

By using the relation

$$\Delta F = k_i i_c + (ms^2 + k_\theta)\theta \tag{B24}$$

this system of equations can be put into matrix form as follows:

$$\begin{bmatrix} \Delta F \\ 0 \end{bmatrix} = \begin{bmatrix} ms^2 + k_\theta & k_i \\ \dfrac{k_a k_p [k_g + (k_g + k_r)\tau_2 s]}{(1+\tau_2 s)(1+\tau_1 s)} & -1 \end{bmatrix} \begin{bmatrix} \theta \\ i_c \end{bmatrix} \quad \text{(B25)}$$

Then, solving this matrix formulation of the system dynamic equations for θ gives the following equation for $\theta(s)$:

$$\theta(s) = \frac{\Delta F}{(ms^2 + k_\theta) + \dfrac{k_i k_a k_p [k_g + (k_g + k_r)\tau_2 s]}{(1+\tau_2 s)(1+\tau_1 s)}} \quad \text{(B26)}$$

where

$$\Delta F = k_i i_c + (ms^2 + k_\theta)\theta \quad \text{(B27)}$$

Thus

$$\theta(s) = \frac{k_i i_c + (ms^2 + k_\theta)\theta}{(ms^2 + k_\theta) + \dfrac{k_i k_a k_p [k_g + (k_g + k_r)\tau_2 s]}{(1+\tau_2 s)(1+\tau_1 s)}} \quad \text{(B28)}$$

Setting this relation equal to the lumped second-order system of a spring dashpot configuration gives the theoretical stiffness and damping values for the closed-loop magnetic circuit configuration:

$$\theta(j\omega) = \frac{k_i i_c + (k_\theta - m\omega^2)\theta}{(k_\theta - m\omega^2) + \dfrac{k_i k_a k_p [k_g + (k_g + k_r)\tau_2 j\omega]}{(1+\tau_2 j\omega)(1+\tau_1 j\omega)}}$$

$$= \frac{f(\omega)}{(k_{eq} - m\omega^2) + j\omega c_{eq}} \quad \text{(B29)}$$

Thus, from the equality given in equation (B29), one obtains the following relations:

$$f(\omega) = k_i i_c + (k_\theta - m\omega^2)\theta \quad \text{(B30)}$$

$$k_{eq} = k_\theta + \mathcal{R}e \left\{ \frac{k_i k_a k_p [k_g + (k_g + k_r)\tau_2 j\omega]}{(1+\tau_2 j\omega)(1+\tau_1 j\omega)} \right\} \quad \text{(B31)}$$

and

$$c_{eq} = \frac{\mathcal{I}m}{\omega} \left\{ \frac{k_i k_a k_p [k_g + (k_g + k_r)\tau_2 j\omega]}{(1+\tau_2 j\omega)(1+\tau_1 j\omega)} \right\} \quad \text{(B32)}$$

Therefore, evaluating the equivalent stiffness and damping for the closed-loop system gives the following relations:

$$k_{eq} = k_\theta + \frac{k_i k_a k_p [k_g (1 - \tau_2 \tau_1 \omega^2) + (k_g + k_r)(\tau_2 + \tau_1)\tau_2 \omega^2]}{(1 - \tau_2 \tau_1 \omega^2)^2 + (\tau_2 + \tau_1)^2 \omega^2} \quad \text{(B33)}$$

$$c_{eq} = \frac{k_i k_a k_p [(1 - \tau_2 \tau_1 \omega^2)(k_g + k_r)\tau_2 - k_g(\tau_2 + \tau_1)]}{(1 - \tau_2 \tau_1 \omega^2)^2 + (\tau_2 + \tau_1)^2 \omega^2} \quad \text{(B34)}$$

Appendix C
Theoretical Evaluation of Several Active Feedback Methods

The following analysis supports the background summary of the inertial isolation techniques which, with the needed relative support information, lead to the prototype design. The approach taken for the response analysis on these one-degree-of-freedom, inertially based isolation systems was based on work by D. Schubert, Barry Controls Eastern Operation, Barry Wright Corporation, Watertown, Massachusetts. Three physical models (fig. 13) will be analyzed to characterize isolation with acceleration, velocity, and both acceleration and velocity as the control feedback signals.

For the physical systems described in figure 13, two system disturbances exist. The first is the base motion or a structural excitation **u**. The second is an applied force **F** to the payload mass m. Both terms **u** and **F** are considered to be functions for which Laplace transformations can be realized. The isolator force $\mathbf{F}_s$ on the active control configurations is generated by sensing velocity, acceleration, or both, and driving an actuator out of phase with the control signal.

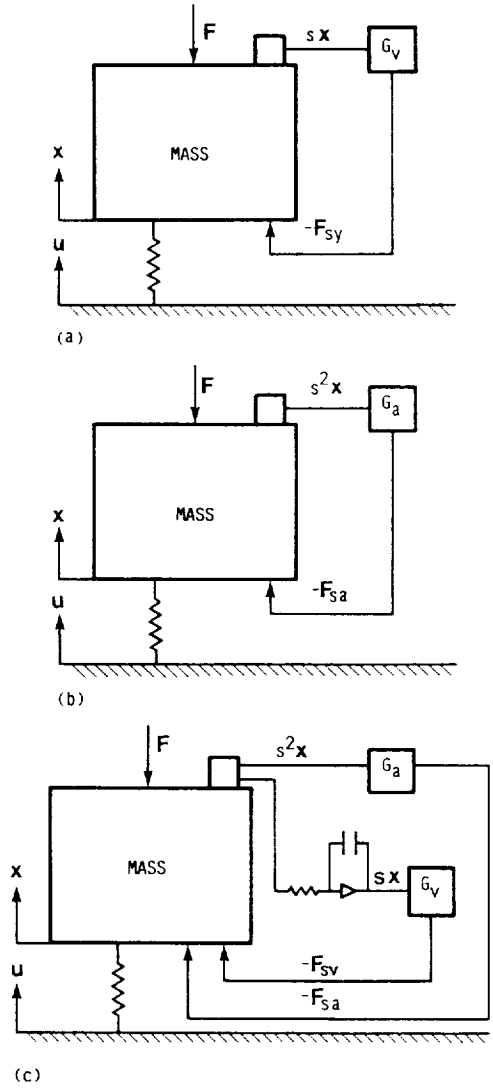

(a) Velocity feedback.
(b) Acceleration feedback.
(c) Acceleration and velocity feedback.

Figure 13.—Physical description of three one-degree-of-freedom inertial isolation configurations.

The sensor function is to convert the velocity $d\mathbf{x}/dt$ of the payload (or acceleration $d^2\mathbf{x}/dt^2$) into an electrical voltage proportional to the excitation. The sensor output voltage E_v is proportional to velocity $d\mathbf{x}/dt$ (or acceleration $d^2\mathbf{x}/dt^2$) such that $E_{vv} = A_v d\mathbf{x}/dt$ (or $E_{va} = A_a d^2\mathbf{x}/dt$). The voltage E_v is amplified with gain B_v (*or* B_a), such that the output voltage from the amplifier E_{avv} (or E_{ava}) is $E_{avv} = A_v B_v d\mathbf{x}/dt$ (or $E_{ava} = A_a B_a d^2\mathbf{x}/dt^2$). The voltage is then applied to a Lorentz force actuator coil of resistance $R(\Omega)$ having negligible inductance. This coil is immersed in a magnetic field having a field strength ψ. Application of the voltage to the coil produces a current having magnitude $I_{avv} = E_{avv}/R$ (or $I_{ava} = E_{ava}/R$). The effect of the current flowing through a coil of N turns of wire results in a force F_s, where $F_{sv} = \psi N I_{avv}$ (or $F_{sa} = \psi N I_{ava}$). To simplify this, a gain term G_v (or G_a) is applied to the feedback signal. This gain term relates the velocity $d\mathbf{x}/dt$ (or acceleration $d^2\mathbf{x}/dt^2$) to the force $\mathbf{F}_{sv}$ (or $\mathbf{F}_{sa}$) such that $\mathbf{F}_{sv} = G_v d\mathbf{x}/dt$ (or $\mathbf{F}_{sa} = G_a d^2\mathbf{x}/dt^2$). Now $\mathbf{F}_{sv} = -G_v d\mathbf{x}/dt$ and $\mathbf{F}_{sa} = -G_a d^2\mathbf{x}/dt^2$, where the negative sign denotes negative feedback. The sign applied to the isolator force term $\mathbf{F}_s$ is governed by the direction the servo current flows through the coil of wire.

The equations to model the three isolation systems are as follows. The differential equation of motion for the active isolation systems is obtained from the force balance method by using Newton's first and second laws. Here the base motion **u** is actually a time function, so that $\mathbf{u} = \mathbf{u}(t)$, and the applied force **F** is, in actuality, $\mathbf{F}(t)$. Thus, for velocity feedback,

$$m\frac{d^2\mathbf{x}}{dt^2} = \mathbf{F} + \mathbf{F}_{sv} + K(\mathbf{u}-\mathbf{x}) \tag{C1}$$

Substituting and rearranging give the following equations:

$$m\frac{d^2\mathbf{x}}{dt^2} = F - G_v\frac{d\mathbf{x}}{dt} + K(\mathbf{u}-\mathbf{x}) \tag{C2}$$

$$m\frac{d^2\mathbf{x}}{dt^2} + G_v\frac{d\mathbf{x}}{dt} + K\mathbf{x} = F + K\mathbf{u} \tag{C3}$$

For acceleration feedback,

$$m\frac{d^2\mathbf{x}}{dt^2} = \mathbf{F} + \mathbf{F}_{sa} + K(\mathbf{u}-\mathbf{x}) \tag{C4}$$

Substituting and rearranging give the following equations:

$$m\frac{d^2\mathbf{x}}{dt^2} = \mathbf{F} - G_a\frac{d^2\mathbf{x}}{dt^2} + K(\mathbf{u}-\mathbf{x}) \tag{C5}$$

$$m\frac{d^2\mathbf{x}}{dt^2} + G_a\frac{d^2\mathbf{x}}{dt^2} + K\mathbf{x} = \mathbf{F} + K\mathbf{u} \tag{C6}$$

For acceleration and velocity feedback,

$$m\frac{d^2\mathbf{x}}{dt^2} = \mathbf{F} + \mathbf{F}_{sa} + \mathbf{F}_{sv} + K(\mathbf{u}-\mathbf{x}) \tag{C7}$$

Substituting and rearranging give the following equations:

$$m\frac{d^2\mathbf{x}}{dt^2} = \mathbf{F} - G_a\frac{d^2\mathbf{x}}{dt^2} - G_v\frac{d\mathbf{x}}{dt} + K(\mathbf{u}-\mathbf{x}) \tag{C8}$$

$$m\frac{d^2\mathbf{x}}{dt^2} + G_a\frac{d^2\mathbf{x}}{dt^2} + G_v\frac{d\mathbf{x}}{dt} + K\mathbf{x} = \mathbf{F} + K\mathbf{u} \tag{C9}$$

Base-Excited Vibration Response

To determine the base-excited response for the three vibration isolation systems, the force term $\mathbf{F}(t)$ is set equal to zero. The base displacement term $\mathbf{u}(t)$ is assumed to be a sine wave having a peak amplitude of B. Thus, $\mathbf{u}(t) = B\sin(\omega t)$, where ω is a frequency term. The three equations of motion become, for velocity feedback,

$$m\frac{d^2\mathbf{x}}{dt^2} + G_v\frac{d\mathbf{x}}{dt} + K\mathbf{x} = KB\sin(\omega t) \tag{C10}$$

for acceleration feedback,

$$m\frac{d^2\mathbf{x}}{dt^2} + G_a\frac{d^2\mathbf{x}}{dt^2} + K\mathbf{x} = KB\sin(\omega t) \tag{C11}$$

and for both acceleration and velocity feedback,

$$m\frac{d^2\mathbf{x}}{dt^2} + G_a\frac{d^2\mathbf{x}}{dt^2} + G_v\frac{d\mathbf{x}}{dt} + K\mathbf{x} = KB\sin(\omega t) \tag{C12}$$

The equations are then transformed into the frequency domain by using the Laplace transformation:

$$F(s) = \int_{-\infty}^{\infty} F(t)e^{-st}dt \tag{C13}$$

The velocity system equation becomes

$$ms^2X(s) + G_vsX(s) + KX(s) = KU(s) \tag{C14}$$

the acceleration system equation becomes

$$ms^2X(s) + G_as^2X(s) + KX(s) = KU(s) \tag{C15}$$

and the acceleration and velocity system equation becomes

$$ms^2X(s) + G_as^2X(s) + G_vsX(s) + KX(s) = KU(s) \tag{C16}$$

The base-excited system transfer function is defined as $X(s)/U(s) = T(s)$. Thus, the transfer functions for the three isolation systems are, for velocity feedback,

$$\frac{X(s)}{U(s)} = \frac{K}{ms^2+G_vs+K} \tag{C17}$$

for acceleration feedback,

$$\frac{X(s)}{U(s)} = \frac{K}{ms^2+G_as^2+K} \tag{C18}$$

for both acceleration and velocity feedback,

$$\frac{X(s)}{U(s)} = \frac{K}{ms^2+G_as^2+G_vs+K} \tag{C19}$$

Transforming these transfer functions into a standard vibration notation gives, for velocity feedback,

$$\frac{X}{U}(s) = \frac{\omega_n^2}{s^2+2\xi\omega_n s+\omega_n^2} \tag{C20}$$

for acceleration feedback,

$$\frac{X}{U}(s) = \frac{\omega_n^2}{s^2+\frac{b_2}{s\pi f_o^2}s^2+\omega_n^2} \tag{C21}$$

and for acceleration and velocity feedback,

$$\frac{X}{U}(s) = \frac{\omega_n^2}{s^2+\frac{b_2}{2\pi f_o^2}s^2+2\xi\omega_n s+\omega_n^2} \tag{C22}$$

where $G_a/m = b_2/2\pi f_o^2$, $G_v/m = 2\xi\omega_n$, $\xi = \frac{1}{2}G_v(1/Km)^{1/2}$.

In this form the denominator of each transfer function is called the characteristic equation. If the characteristic equation has real negative roots, the vibration isolation system will not oscillate; if it has complex roots, it will oscillate. If the base motion displacement time function $\mathbf{u}(t)$ is a "pure sinusoid," the steady-state frequency response in complex form is given by letting $s = j\omega$.

Thus, the frequency response is obtained by the function

$$\frac{X}{U}(j\omega) = \lim_{t\to\infty}\left[\frac{X}{U}(s)\right] \tag{C23}$$

where $s = j\omega$ and $j = \sqrt{-1}$. This frequency response, which is a vector, becomes, for velocity feedback,

$$\frac{X}{U}(j\omega) = \frac{\omega_n^2}{(\omega_n^2 - \omega^2) + 2\xi\omega_n j\omega} \tag{C24}$$

for acceleration feedback,

$$\frac{X}{U}(j\omega) = \frac{\omega_n^2}{\omega_n^2 - \left(1 + \dfrac{b_2}{2\pi f_o^2}\right)\omega^2} \tag{C25}$$

and for both acceleration and velocity feedback,

$$\frac{X}{U}(j\omega) = \frac{\omega_n^2}{\left[\omega_n^2 - \left(1 + \dfrac{b_2}{2\pi f_o^2}\right)\omega^2\right] + 2\xi\omega_n j\omega} \tag{C26}$$

The magnitude of vibration measured on the isolated payload resulting from the sinusoidal excitation $B\sin(\omega t)$ is the vector of length $|X(j\omega)/U(j\omega)|$. This value, called the transmissibility, is a scalar since the phase angle is not used. It is generally written as $T(j\omega) = |X(j\omega)/U(j\omega)|$. Thus, the transmissibility function for the systems of interest become, for velocity feedback,

$$T_{av} = \left|\frac{X}{U_{av}}(j\omega)\right| = \left\{\frac{1}{\left[1 - \left(\dfrac{\omega}{\omega_n}\right)^2\right]^2 + \left(2\xi\dfrac{\omega}{\omega_n}\right)^2}\right\}^{1/2} \tag{C27}$$

for acceleration feedback,

$$T_{aa} = \left|\frac{X}{U_{aa}}(j\omega)\right| = \frac{1}{1 - \left(1 + \dfrac{b_2}{2\pi f_o^2}\right)\left(\dfrac{\omega}{\omega_n}\right)^2} \tag{C28}$$

and for both acceleration and velocity feedback,

$$T_{aav} = \left|\frac{X}{U_{aav}}(j\omega)\right| = \left\{\frac{1}{\left[1 - \left(1 + \dfrac{b_2}{2\pi f_o^2}\right)\left(\dfrac{\omega}{\omega_n}\right)^2\right]^2 + \left(2\xi\dfrac{\omega}{\omega_n}\right)^2}\right\}^{1/2} \tag{C29}$$

The data shown in figures 14 to 16 present transmissibility versus nondimensional frequency as functions of the damping term ξ and the acceleration term $b_2/2\pi f_o^2$.

Force-Excited Vibration Response

Motion of the isolated payload can result from two excitation sources. The first is base motion. The second results from external forces applied directly to the isolated payload. Referring back to the first differential equations of motion (C3), (C6), and (C9), and setting the base excitation term $\mathbf{u}(t)$ to zero allows the external force $\mathbf{F}(t)$ to excite the payload. The equations of motion are, for velocity feedback,

$$m\frac{d^2\mathbf{x}}{dt^2} = \mathbf{F}(t) - \mathbf{F}_{sv} - K\mathbf{x} \tag{C30}$$

for acceleration feedback,

$$m\frac{d^2\mathbf{x}}{dt^2} = \mathbf{F}(t) - \mathbf{F}_{sa} - K\mathbf{x} \tag{C31}$$

and for both acceleration and velocity feedback,

$$m\frac{d^2\mathbf{x}}{dt^2} = \mathbf{F}(t) - \mathbf{F}_{sa} - \mathbf{F}_{sv} - K\mathbf{x} \tag{C32}$$

These equations can be placed in the Laplace operation format for velocity feedback,

$$ms^2X(s) + G_v sX(s) + KX(s) = F(s) \tag{C33}$$

for acceleration feedback,

$$ms^2X(s) + G_a s^2X(s) + KX(s) = F(s) \tag{C34}$$

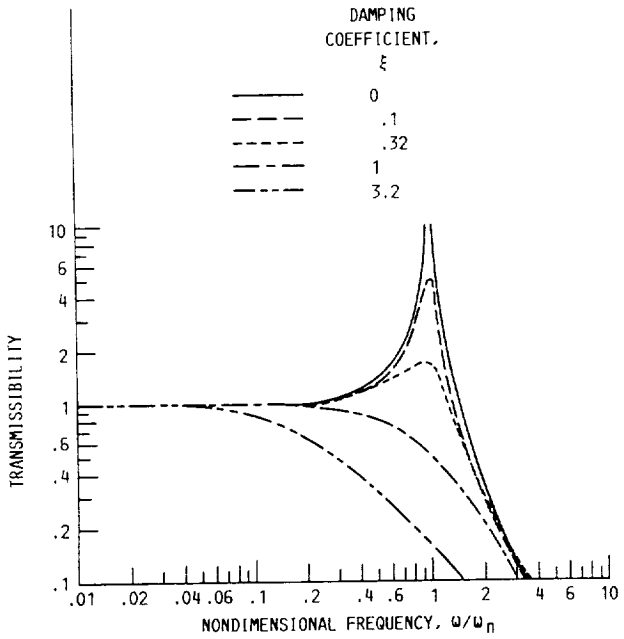

Figure 14.—Inertial velocity feedback transmissibility curves.

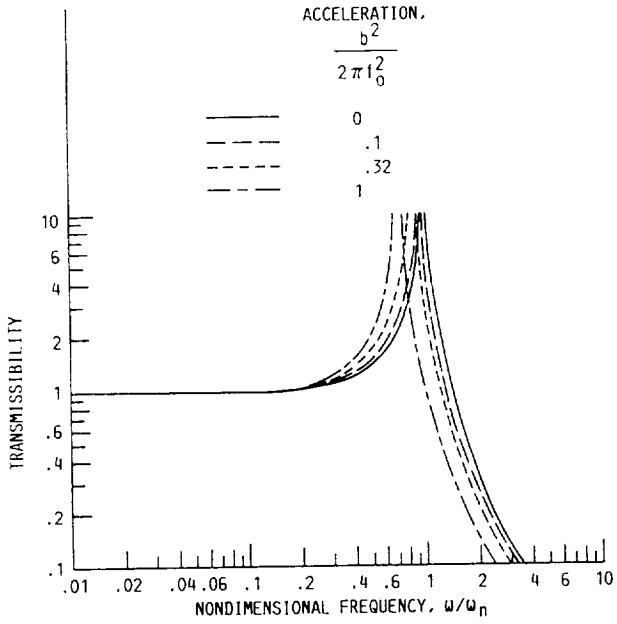

Figure 15.—Inertial acceleration feedback transmissibility curves.

and for both acceleration and velocity feedback,

$$ms^2X(s) + G_a s^2 X(s) + G_v sX(s) + KX(s) = F(s) \quad \text{(C35)}$$

The sensitivity of the isolated payload to the disturbing force $F(s)$ is characterized by a term called the isolated payload mobility. Mobility is the vector magnitude of $X(s)/F(s)$. Mobility measures the amount by which the payload is deflected per unit of externally applied force. In Laplace notation form, the equations for mobility become, for velocity feedback,

$$\frac{X}{F}(s)_v = \frac{1}{ms^2 + G_v s + K} \quad \text{(C36)}$$

for acceleration feedback,

$$\frac{X}{F}(s)_a = \frac{1}{ms^2 + G_a s^2 + K} \quad \text{(C37)}$$

and for both acceleration and velocity feedback,

$$\frac{X}{F}(s)_{av} = \frac{1}{ms^2 + G_v s + G_a s^2 + K} \quad \text{(C38)}$$

These equations are made nondimensional, as was done for the transmissibility functions, by dividing by the mass m of the isolated payload and defining the following: $\omega_n = (K/m)^{1/2}$, $\xi = \frac{1}{2}G_v(1/Km)^{1/2}$, and $G_a/m = b_2/2\pi f_o^2$. Making these substitutions gives, for velocity feedback,

$$\frac{X}{F}(s)_v = \frac{1}{s^2 + 2\xi\omega_n s + \omega_n^2} \quad \text{(C39)}$$

for acceleration feedback,

$$\frac{X}{F}(s)_a = \frac{1}{s^2 + \dfrac{b_2}{2\pi f_o^2}\, s^2 + \omega_n^2} \quad \text{(C40)}$$

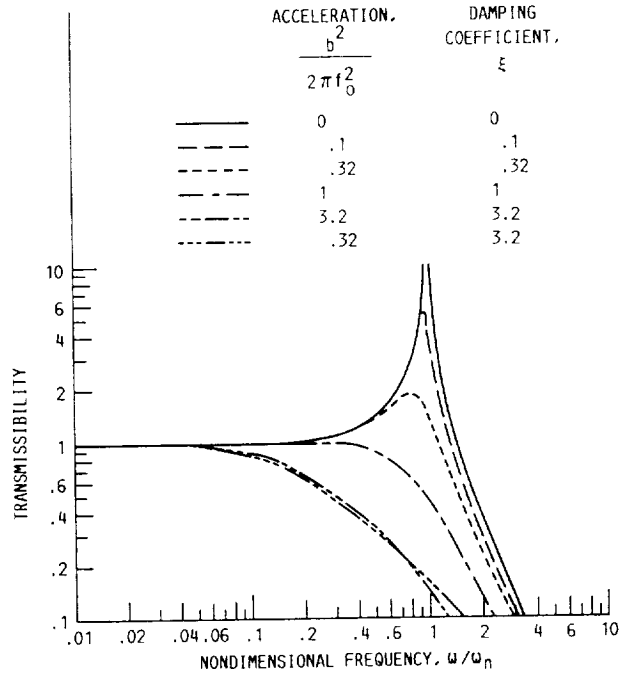

Figure 16.—Inertial acceleration and velocity feedback transmissibility curves.

and for both acceleration and velocity feedback,

$$\frac{X}{\mathbf{F}}(s)_{av} = \frac{1}{s^2 + 2\xi\omega_n s + \frac{b_2}{2\pi f_o^2}\, s^2 + \omega_n^2} \tag{C41}$$

To show the effectiveness of the active systems, the ratio of $X(s)/F(s)$ for an active system to $X(s)/F(s)$ for the passive part of the system is used. This ratio is called the mobility effectiveness $X_f(s)$. Thus, if X_f is unity, then the effectiveness of the active vibration isolation system in reducing force-induced payload motion is zero, or the active portion of the system does nothing. If X_f is zero, then the effectiveness of the active portion of the system is complete, and there is no motion of the isolated payload resulting from a finite applied force. If X_f is greater than unity, then the active portion of the vibration isolation system amplifies the effect of the applied force, giving rise to more payload motion with active feedback than without it. The equations for the effectiveness function for the different systems are, for velocity feedback,

$$X_f(s)_v = \frac{s^2 + 2\xi_1\omega_n s + \omega_n^2}{s^2 + 2\xi\omega_n s + \omega_n^2} \tag{C42}$$

for acceleration feedback,

$$X_f(s)_a = \frac{s^2 + 2\xi_1\omega_n s + \omega_n^2}{s^2 + \frac{b_2}{2\pi f_o^2}\, s^2 + \omega_n^2} \tag{C43}$$

where $\xi_1 = \frac{1}{2}c(1/Km)^{1/2}$, and for both acceleration and velocity feedback,

$$X_f(s)_{av} = \frac{s^2 + 2\xi_1\omega_n s + \omega_n^2}{s^2 + 2\xi\omega_n s + \frac{b_2}{2\pi f_o^2}\, s^2 + \omega_n^2} \tag{C44}$$

In terms of frequency response, the vector length $X_f(s)$ is $|X_f(j\omega)|$. This value is obtained in the same manner as was done for transmissibility. The equations for the effectiveness of the systems become, for velocity feedback,

$$\left| X_f\left(\frac{j\omega}{\omega_n}\right)_v \right| = \left\{ \frac{\left[1 - \left(\frac{\omega}{\omega_n}\right)^2\right]^2 + \left(2\xi_1 \frac{\omega}{\omega_n}\right)^2}{\left[1 - \left(\frac{\omega}{\omega_n}\right)^2\right]^2 + \left(2\xi \frac{\omega}{\omega_n}\right)^2} \right\}^{1/2} \tag{C45}$$

for acceleration feedback,

$$\left| X_f\left(\frac{j\omega}{\omega_n}\right)_a \right| = \left\{ \frac{\left[1 - \left(\frac{\omega}{\omega_n}\right)^2\right]^2 + \left(2\xi_1 \frac{\omega}{\omega_n}\right)^2}{\left[1 - \left(1 + \frac{b_2}{2\pi f_o^2}\right)\left(\frac{\omega}{\omega_n}\right)^2\right]^2} \right\}^{1/2} \tag{C46}$$

and for both acceleration and velocity feedback,

$$\left| X_f\left(\frac{j\omega}{\omega_n}\right)_{av} \right| = \left\{ \frac{\left[1 - \left(\frac{\omega}{\omega_n}\right)^2\right]^2 + \left(2\xi_1 \frac{\omega}{\omega_n}\right)^2}{\left[1 - \left(1 + \frac{b_2}{2\pi f_o^2}\right)\left(\frac{\omega}{\omega_n}\right)^2\right]^2 + \left(2\xi \frac{\omega}{\omega_n}\right)^2} \right\}^{1/2} \tag{C47}$$

Figures 17 to 19 represent the effectiveness of the force-actuated vibration isolation systems for a passive damping ratio of 0.05, which is typical of spring elements made of steel. The figures show the effectiveness term $|X_f(j\omega)|$ as a function of the nondimensional gain terms.

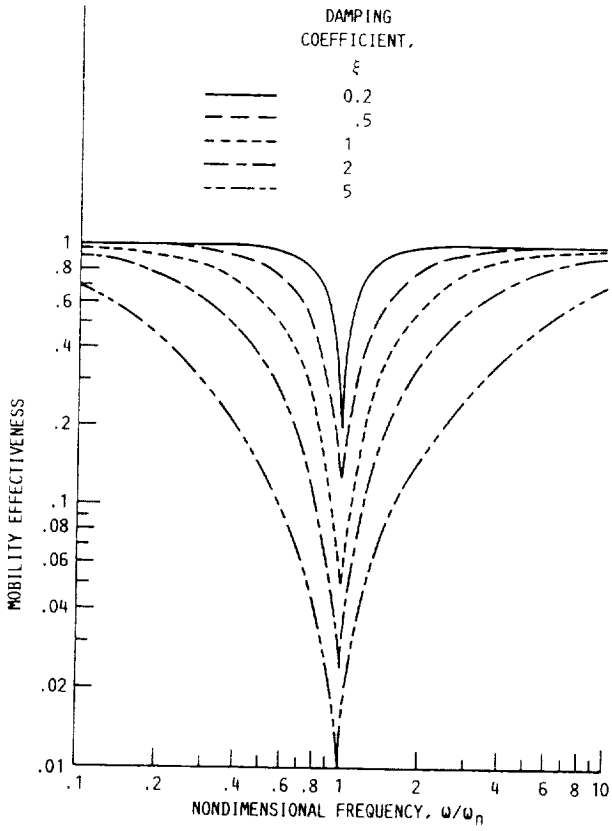

Figure 17.—Inertial velocity feedback mobility curves.

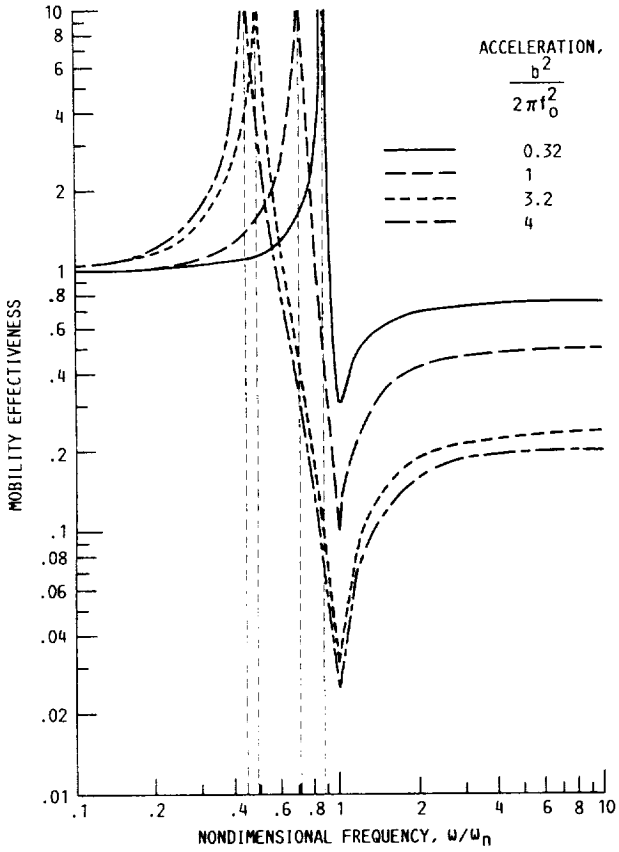

Figure 18.—Inertial acceleration feedback mobility curves.

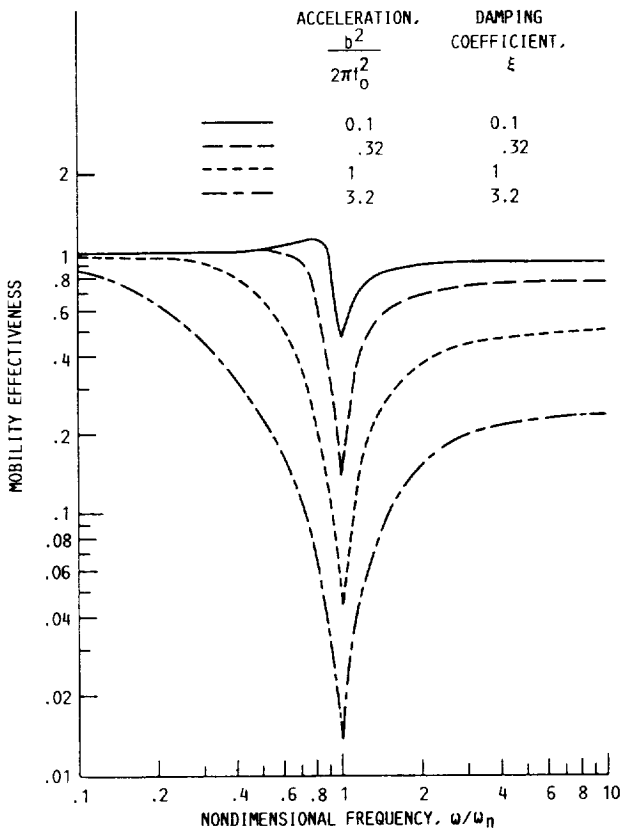

Figure 19.—Inertial acceleration and velocity feedback mobility curves.

References

1. Hamacher, H.: Simulation of Weightlessness. Materials Sciences in Space, B. Feuerbacher, H. Hamacher, and R.J. Naumann, eds., Springer-Verlag, New York, 1986, pp. 31-51.
2. Mitchell, R.A.K., et al., eds.: Measurement and Characterization of the Acceleration Environment on Board the Space Station. Guntersville, AL, Aug. 11-14, 1986, Teledyne Brown Engineering, Huntsville, AL.
3. Jones, D.I., et al.: Microgravity Isolation Mount. ESA-CR(P)-2480, European Space Agency, Paris, France, 1987.
4. Ruzicka, J.E.: Active Vibration and Shock Isolation. SAE Paper 680747, Oct. 1968.
5. Hamacher, H.; Feuerbacher, B.; and Jilg, R.: Analysis of Microgravity Measurements in Spacelab. Fifteenth International Symposium on Space Technology and Science, Vol. 2, H. Matsuo, ed., AGNE Publishing Inc., Tokyo, Japan, 1986, pp. 2087–2097.
6. Humphris, R.R., et al.: Effect of Control Algorithms on Magnetic Journal Bearing Properties. J. Eng. Gas Turbines Power, vol. 108, no. 4, Oct. 1986, pp. 624–632.

NASA
National Aeronautics and Space Administration

Report Documentation Page

1. Report No.	2. Government Accession No.	3. Recipient's Catalog No.
NASA TP-2984		

4. Title and Subtitle	5. Report Date
Development and Approach to Low-Frequency Microgravity Isolation Systems	August 1990
	6. Performing Organization Code

7. Author(s)	8. Performing Organization Report No.
Carlos M. Grodsinsky	E-5287
	10. Work Unit No. 694-03-03

9. Performing Organization Name and Address	11. Contract or Grant No.
National Aeronautics and Space Administration Lewis Research Center Cleveland, Ohio 44135-3191	
	13. Type of Report and Period Covered: Technical Paper

12. Sponsoring Agency Name and Address	14. Sponsoring Agency Code
National Aeronautics and Space Administration Washington, D.C. 20546-0001	

15. Supplementary Notes

16. Abstract

The low-gravity environment provided by space flight has afforded the science community a unique arena for the study of fundamental and technological sciences. However, the dynamic environment observed on space shuttle flights and predicted for Space Station Freedom has complicated the analysis of prior "microgravity" experiments and prompted concern for the viability of proposed space experiments requiring long-term, low-gravity environments. Thus isolation systems capable of providing significant improvements to this random environment are being developed. This report deals with the design constraints imposed by acceleration-sensitive, "microgravity" experiment payloads in the unique environment of space and gives a theoretical background for active isolation. A design is presented for a six-degree-of-freedom, active inertial isolation system based on the baseline relative and inertial isolation techniques described.

17. Key Words (Suggested by Author(s))	18. Distribution Statement
Vibration isolators; Vibration damping; Microgravity experiments; Active; Adaptive control; Electromagnetic	Unclassified – Unlimited Subject Category 31

19. Security Classif. (of this report)	20. Security Classif. (of this page)	21. No. of pages	22. Price*
Unclassified	Unclassified	24	A03

NASA FORM 1626 OCT 86

*For sale by the National Technical Information Service, Springfield, Virginia 22161

NASA-Langley, 1990

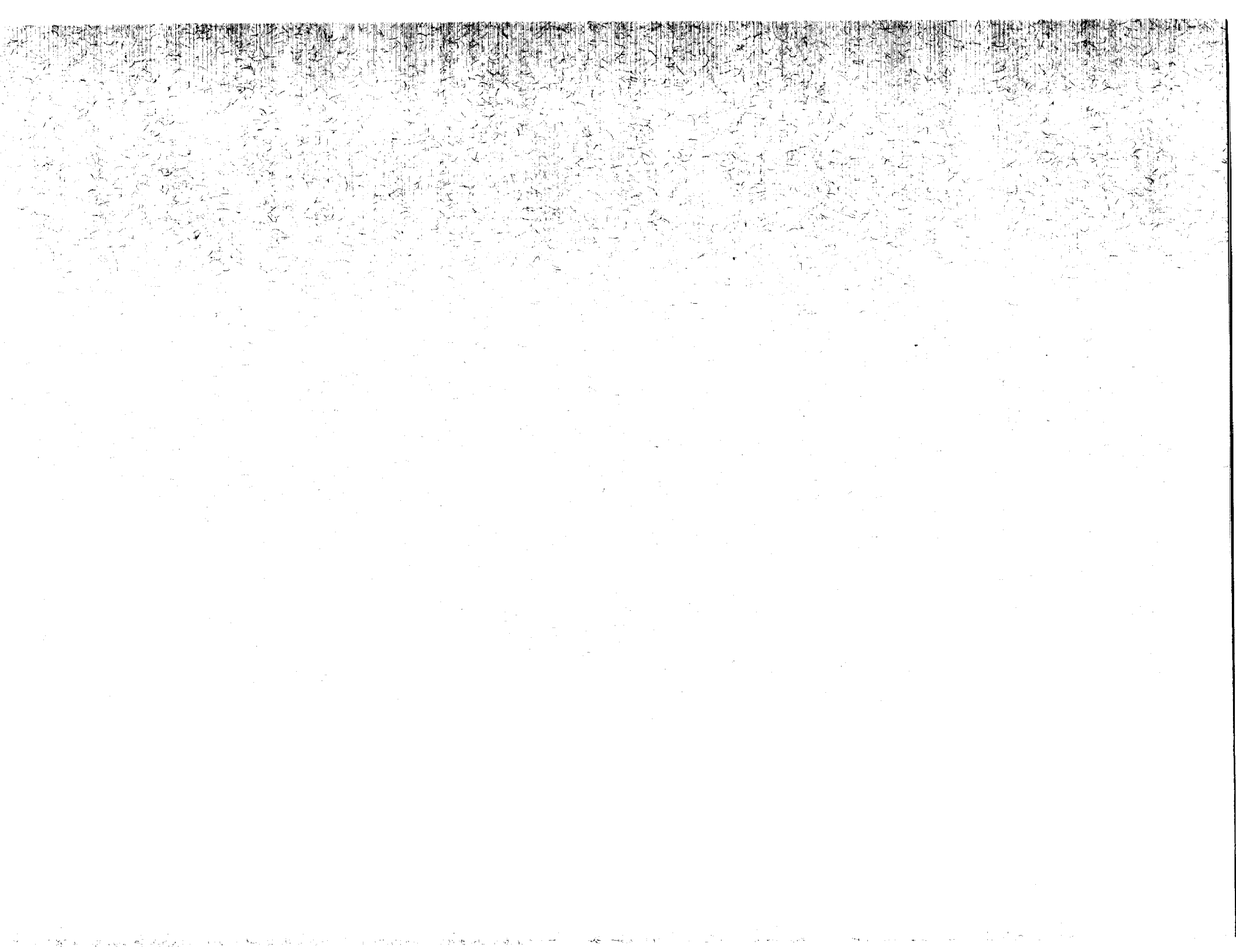

National Aeronautics and
Space Administration
Code NTT-4
Washington, D.C.
20546-0001

Official Business
Penalty for Private Use, $300

BULK RATE
POSTAGE & FEES PAID
NASA
Permit No. G-27

NASA

POSTMASTER: If Undeliverable (Section 158
Postal Manual) Do Not Return